Supporting Information for

3D architectures with $Co_2(OH)_2CO_3$ nanowires wrapped by reduced graphene oxide as superior rate anode materials for Li-ion batteries

Yutao Dong, Yuhang Ma, Yongsheng Li, Meiting Niu, Jie Yang, Xuechao Song, Dan Li, Yushan Liu and Jianmin Zhang*

College of Chemistry and Molecular Engineering

Zhengzhou University

Zhengzhou 450001, China

*Correspondence: zhjm@zzu.edu.cn

Experimental section

Chemicals: Natural graphite flakes with the average diameter of 200 meshes were purchased from Sigma-Aldrich Co. Ltd. (USA), $CoCl_2·6H_2O$, urea, lithium carbonate (Li_2CO_3), tricobalt tetraoxide (Co_3O_4, d=30-50nm), N-methyl-2-pyrrolidinone (NMP), potassium permanganate ($KMnO_4$), hydrogen peroxide (H_2O_2), hydrochloric acid (HCl, 37%) and concentrated sulphuric acid (H_2SO_4, 98%) were analytical grade reagent received from Sinopharm Chemical Reagent Co. Ltd. (Shanghai, China), and used without any further purification. Deionized water was used throughout.

Synthesis of graphene oxide: Graphene oxide (GO) was synthesized using the following modified Hummer's method as reported.[1, 2]

Fig. S1 The black cylindrical hydrogel pictures of the $Co_2(OH)_2CO_3$/rGO.

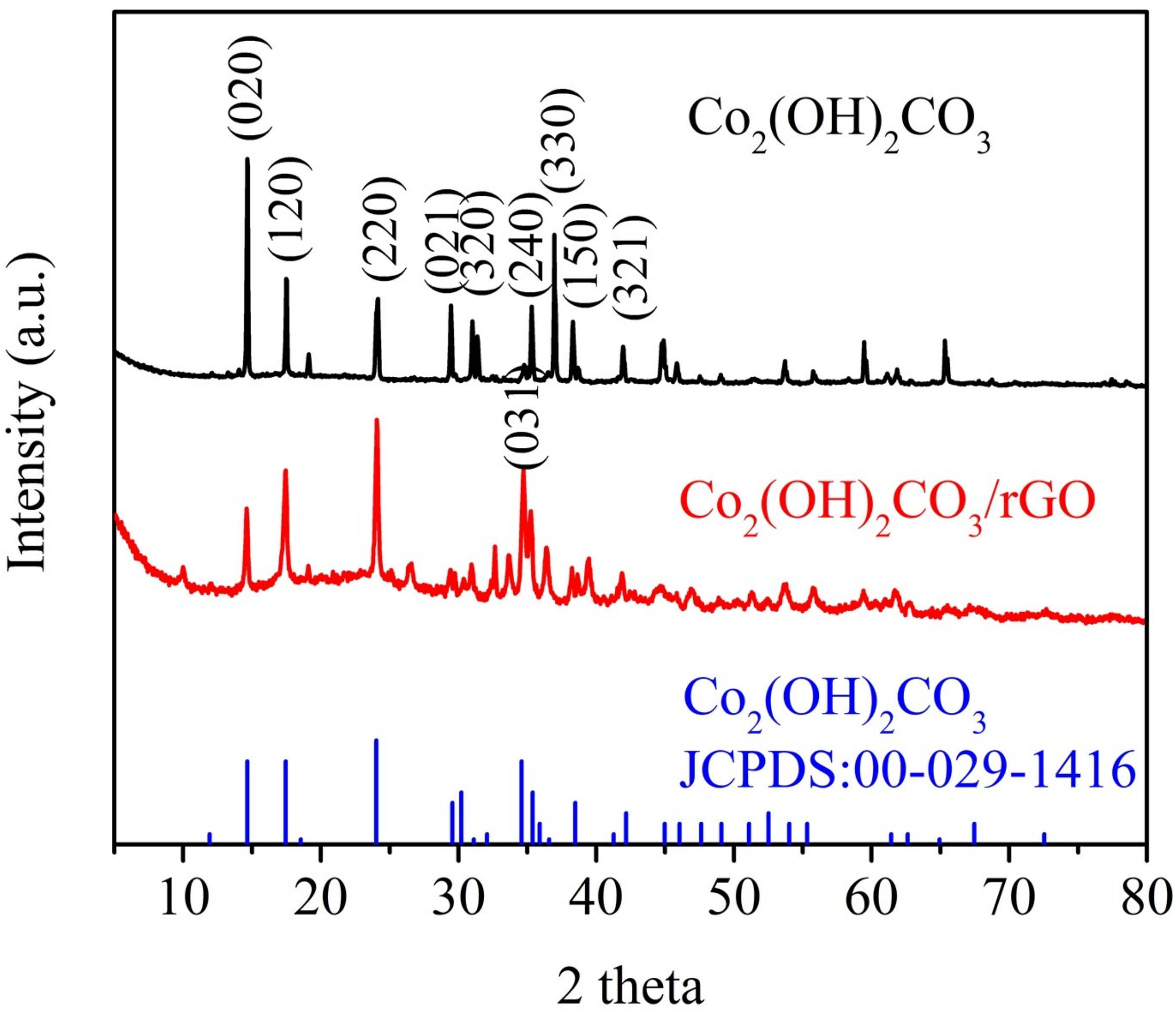

Fig. S2 XRD patterns of the $Co_2(OH)_2CO_3$/rGO and $Co_2(OH)_2CO_3$

Fig. S2 shows the XRD spectra of $Co_2(OH)_2CO_3$/rGO and $Co_2(OH)_2CO_3$ without GO that were prepared in the same hydrothermal environment. For $Co_2(OH)_2CO_3$ and $Co_2(OH)_2CO_3$/rGO, the diffraction peak correspond to the monoclinic standard $Co_2(OH)_2CO_3$ (JCPDS No. 29-1416), and its peak shape is sharp, indicating the $Co_2(OH)_2CO_3$ and $Co_2(OH)_2CO_3$/rGO are high purity and good crystallization, and 10° and 25.7° (002) are rGO diffraction peaks. However, the main crystal plane of $Co_2(OH)_2CO_3$ is (020) crystal plane, and $Co_2(OH)_2CO_3$/rGO is (220) crystal plane. This indicates that the graphene oxide also affects crystal growth of $Co_2(OH)_2CO_3$.

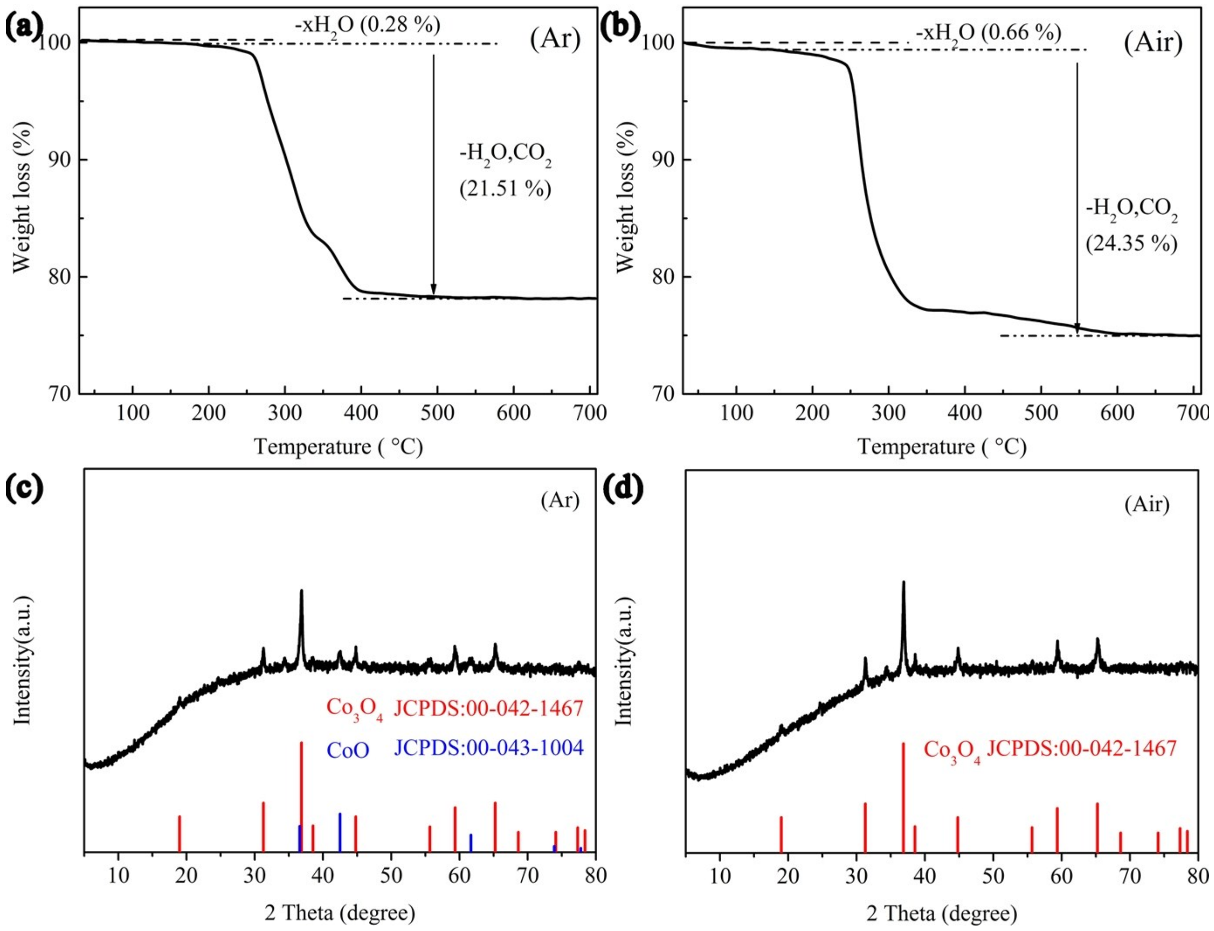

Fig. S3 (a, b) TGA profiles and (c, d) XRD patterns in Ar and air atmosphere of the $Co_2(OH)_2CO_3$ without GO.

As shown in Fig.S3a (in Ar) and Fig.S3b (in air), the two curves exhibit almost the same two successive declining stages, corresponding to the dehydration and dehydration/decarboxylation processes, respectively. The possible processes in argon atmosphere can be demonstrated as following:

$$Co_2(OH)_2CO_3 \cdot xH_2O \overset{\Delta}{\rightarrow} Co_2(OH)_2CO_3 + xH_2O\uparrow(\leq 150℃) \qquad (1)$$

$$2Co_2(OH)_2CO_3 \overset{\Delta}{\rightarrow} CoO + Co_3O_4 + 2H_2O\uparrow + CO\uparrow + CO_2\uparrow(150-500℃\ (in\ Ar)) \quad (2)$$

According to Fig. S3a and b, the first stage occurs below 150℃ with a weight loss of about 0.28 wt.% (Fig. S3a) and 0.66 wt.% (Fig. S3b). It can be belonged to the removal of physically adsorbed water (equation 1). The subsequent weight loss stage is located in the temperature range of 150-500℃, with the weight loss of about 21.51 wt.% (Fig. S3a) and 24.35 wt.% (Fig. S3b). It can be ascribed to the decomposition of $Co_2(OH)_2CO_3$ to cobalt oxide and CO_x. Particularly, the weight have almost no change in the range from 500℃ to 700℃. Moreover, the XRD patterns of the $Co_2(OH)_2CO_3$ after TGA test present the mixture of cubic CoO and Co_3O_4 in Ar and Co_3O_4 in air (Fig. S3c,d).

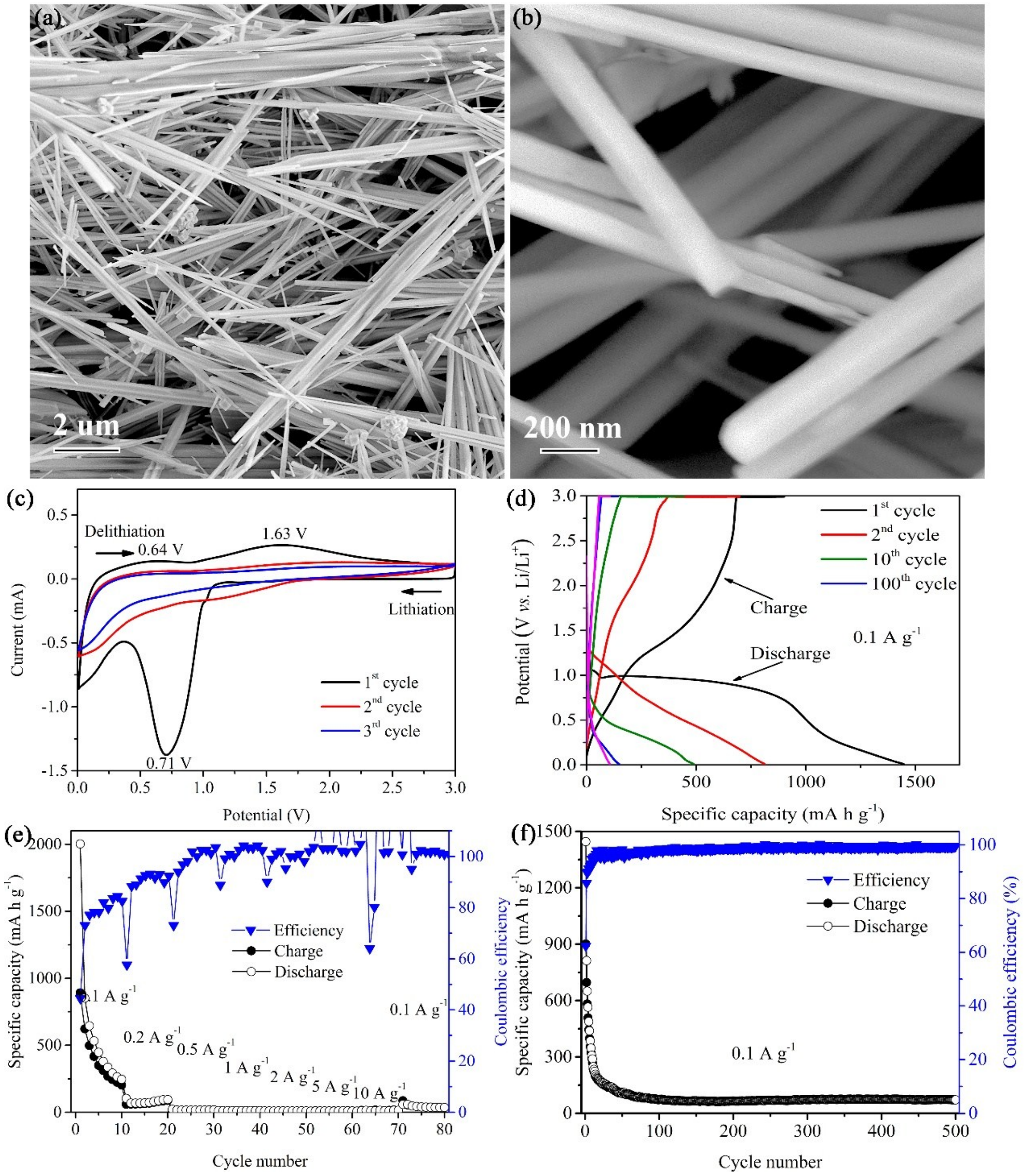

Fig. S4 Characterization and electrochemical performances of $Co_2(OH)_2CO_3$ materials. (a and b) SEM images; (c) cyclic voltammograms recorded at a scan rate of 0.1 mV s^{-1}; (d) Galvanostatic discharge/charge profiles at different rates (increased from 0.1 A g^{-1} to 40 A g^{-1}); (e) rate capability at various current densities (from 0.1 A g^{-1} to 10 A g^{-1}); (f) cycling performance at a current density of 0.1 A g^{-1}.

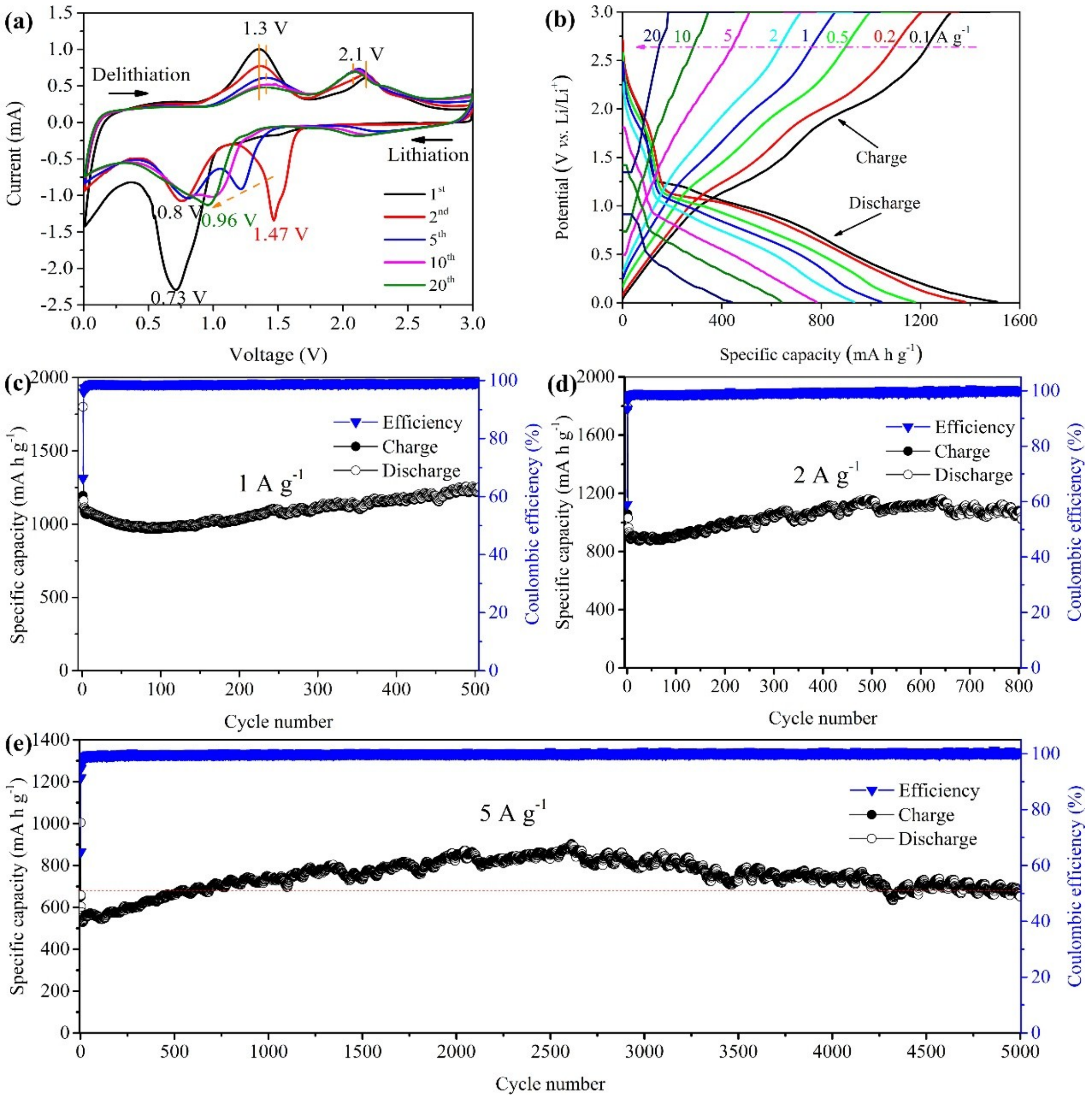

Fig. S5 Electrochemical performances of the $Co_2(OH)_2CO_3$/rGO electrodes. (a) Cyclic voltammograms recorded at a sweep rate of 0.2 mV s^{-1} (0.01 V-3 V), (b) voltage–capacity curves at different rates (increased from 0.1 A g^{-1} to 20 A g^{-1}); (c, d and e) cycling performances at the current densities of 1, 2 and 5 A g^{-1}, respectively.

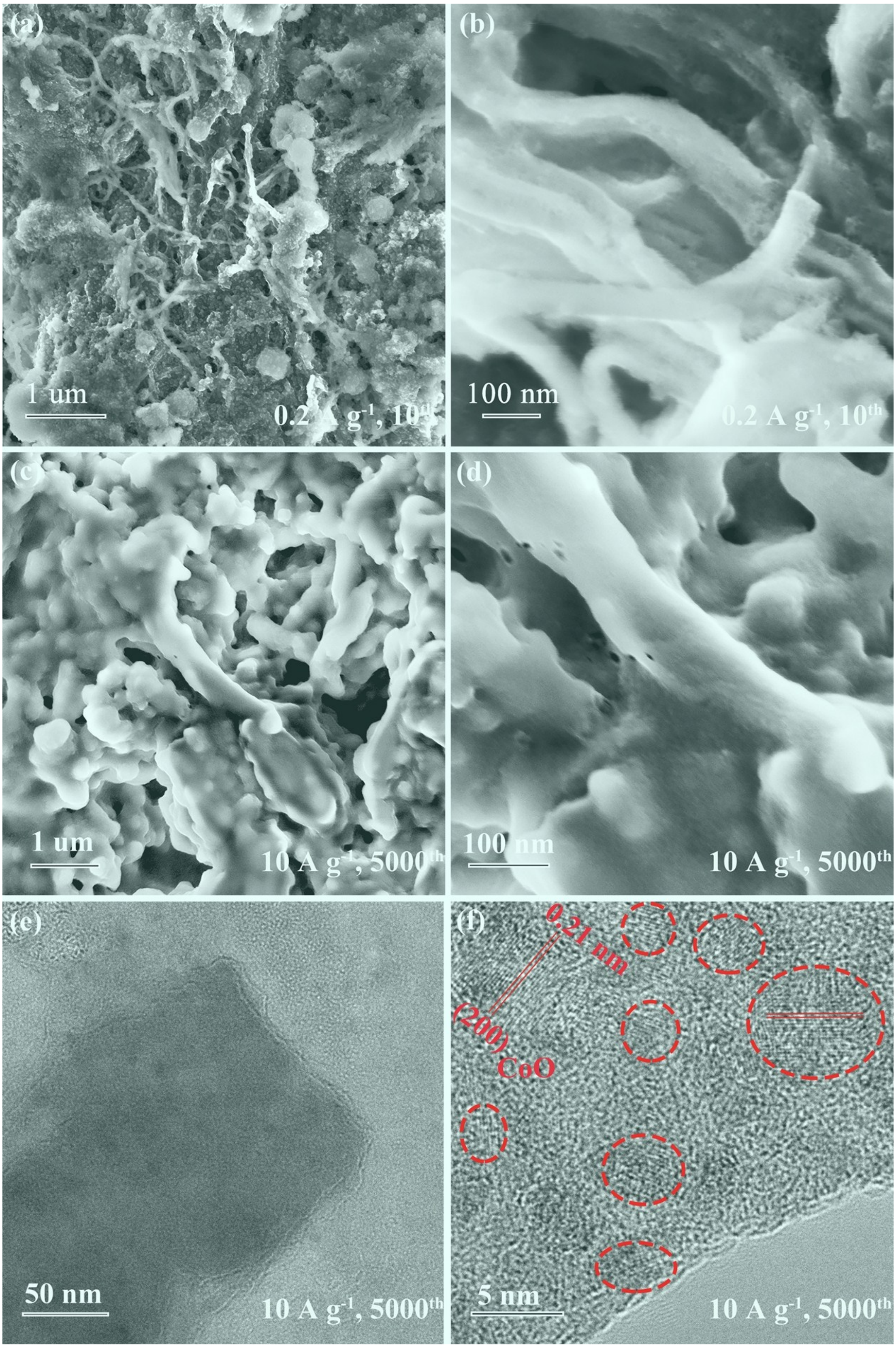

Fig. S6 (a-d) SEM and (e, f) HR-TEM images of the cycled $Co_2(OH)_2CO_3$/rGO electrodes.

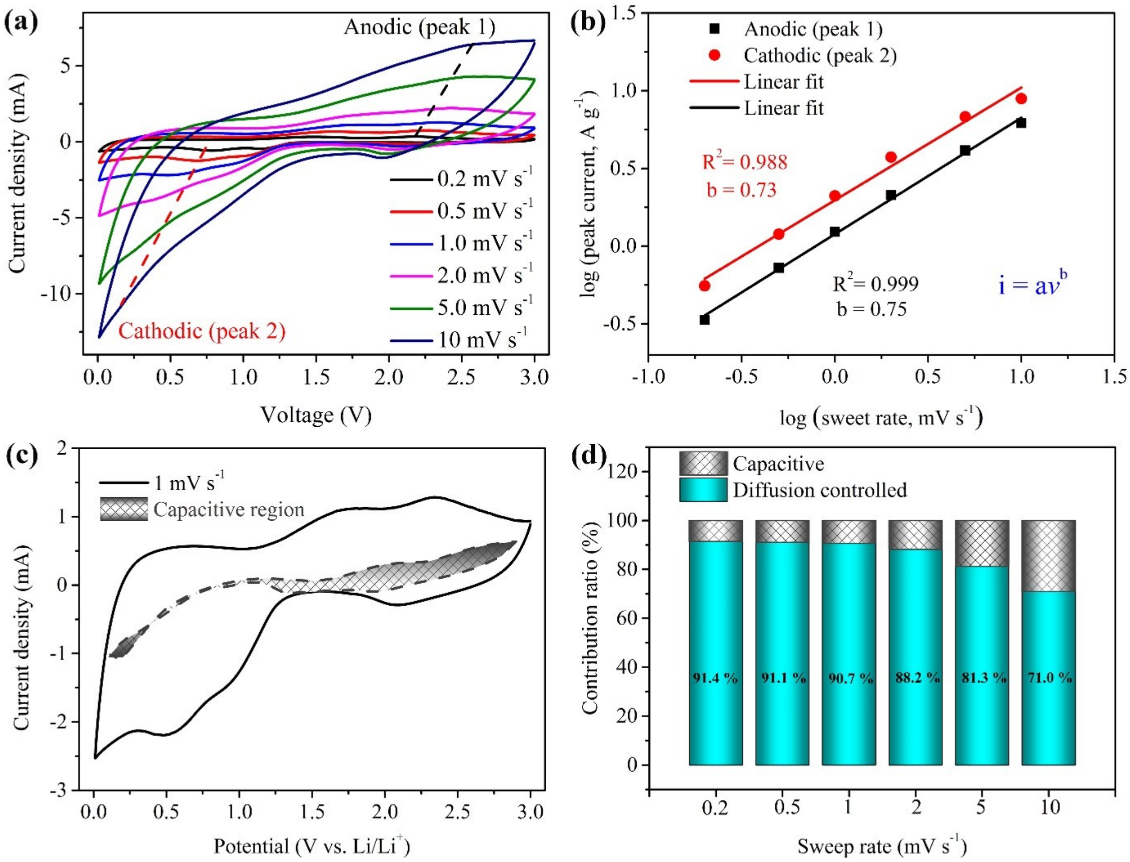

Fig. S7 Electrochemical properties of the $Co_2(OH)_2CO_3$/rGO electrodes. (a) CV curves at various sweep rates from 0.2 to 10 mVs^{-1}; (b) Variation of charge and discharge peak currents with scan rates; (c) Voltammetric response at a scan rate of 1 mV s^{-1}, the capacitive contribution to the total current is shown by the shaded region, and (d) bar chart showing the contribution ratio of diffusion controlled (dark cyan) and capacitive contribution (shade region) at various sweep rates.

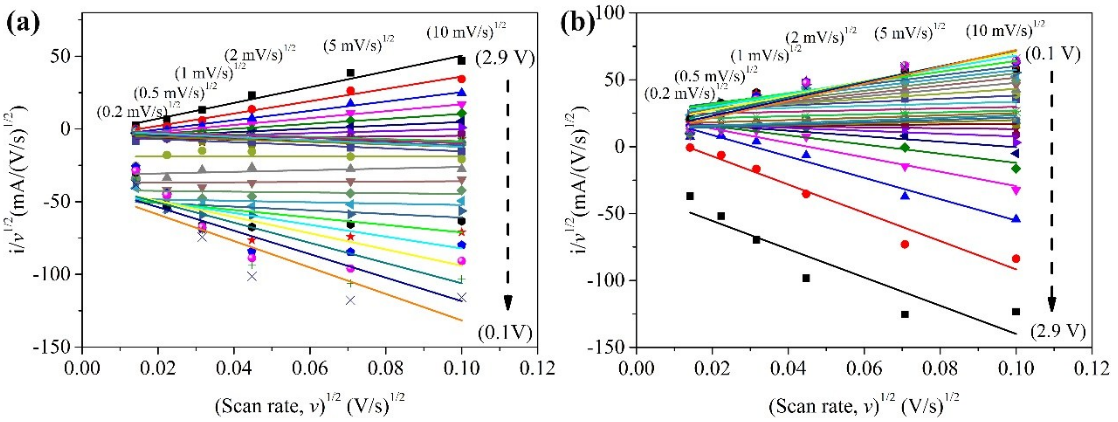

Fig. S8 Charts of the correlation between the $v^{1/2}$ and $i/ v^{1/2}$. Use of equation $i(V) / v^{1/2}) = k_1 v^{1/2} + k_2$ to analyze the (a) cathodic and (b) anodic voltammetric sweep data for the $Co_2(OH)_2CO_3$/rGO electrode: The voltage windows were chose from 2.9 V to 0.1 V (voltage interval is 0.1 volts) and the sweep rates were varied from 0.2 to 10 mV s^{-1}.

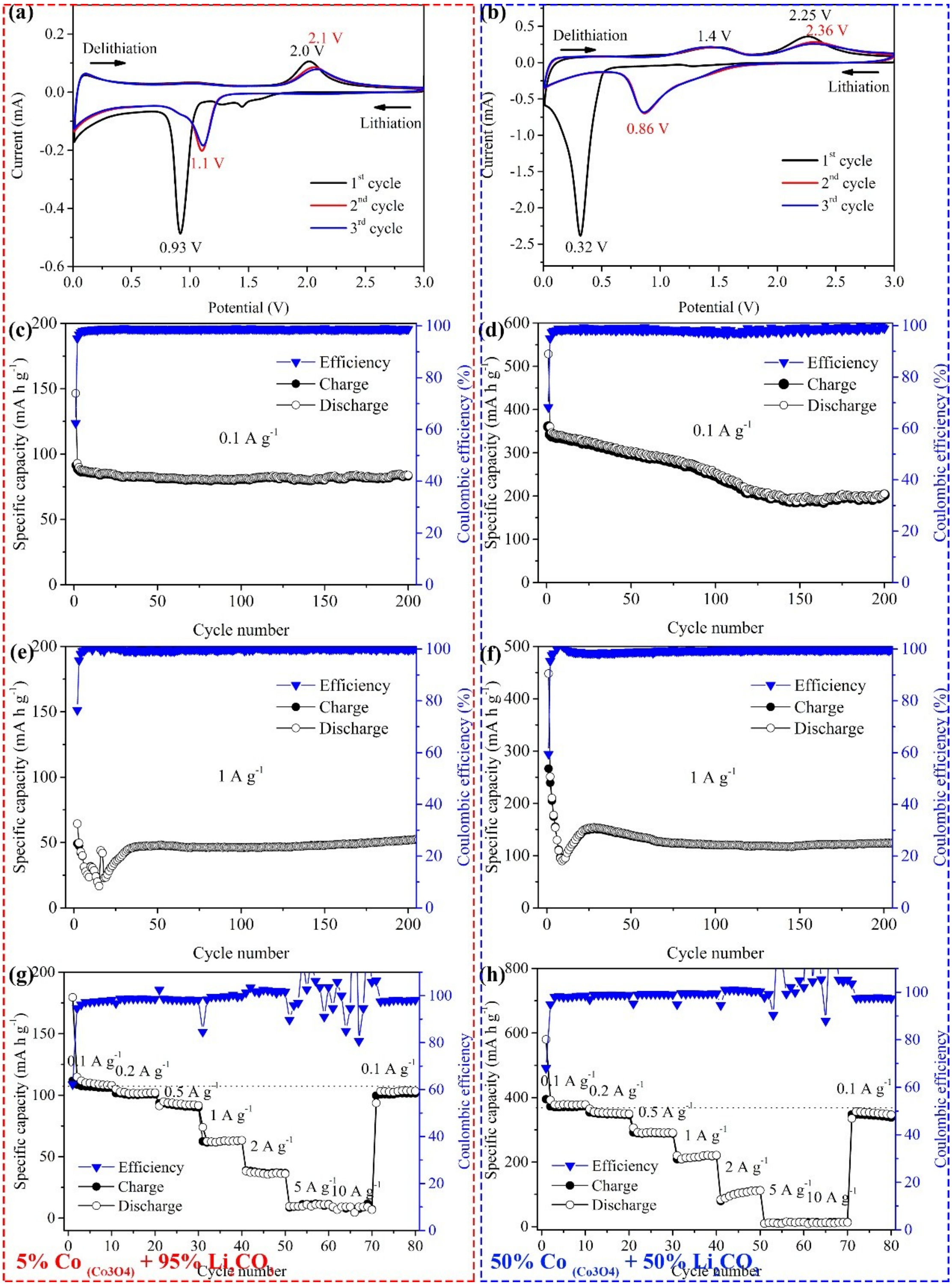

Fig. S9 Electrochemical performance of the mixtures of nano-tricobalt tetraoxide and lithium carbonate at different proportions. (a and b) Cyclic voltammograms recorded at a scan rate of 0.1 mV s^{-1}; (c, d, e and f) cycling performances and (g and h) rate capabilities for the mixtures at various proportions.

Fig. S10 Schematic diagram of battery for in-situ XRD

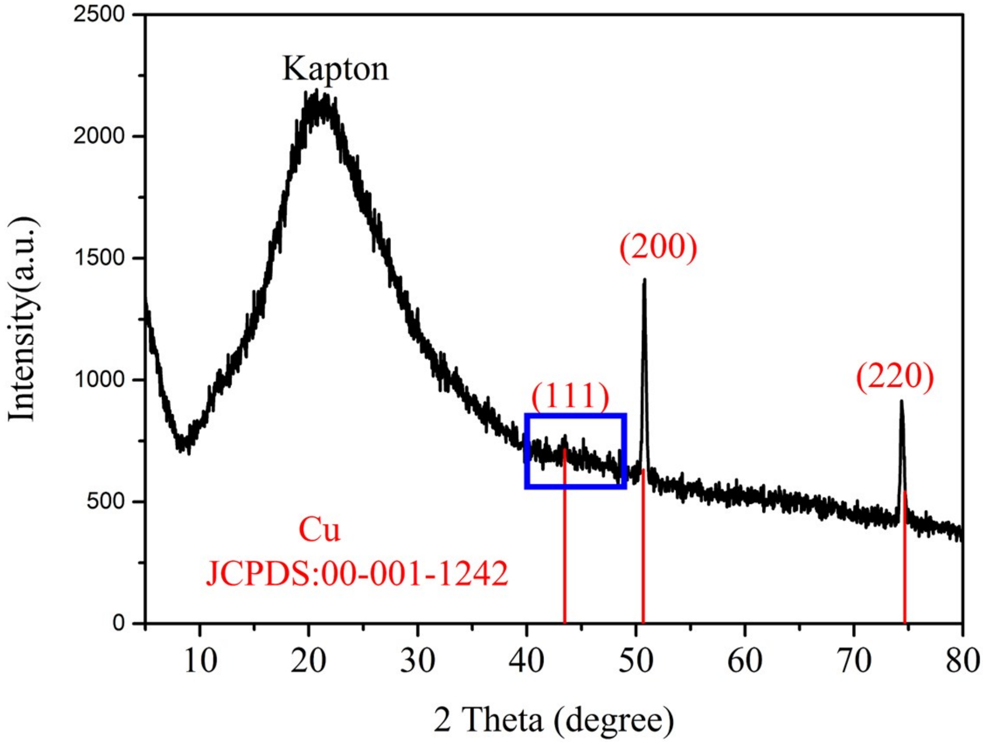

Fig. S11 XRD patterns of ultra-thin copper foil film@Kapton tape.

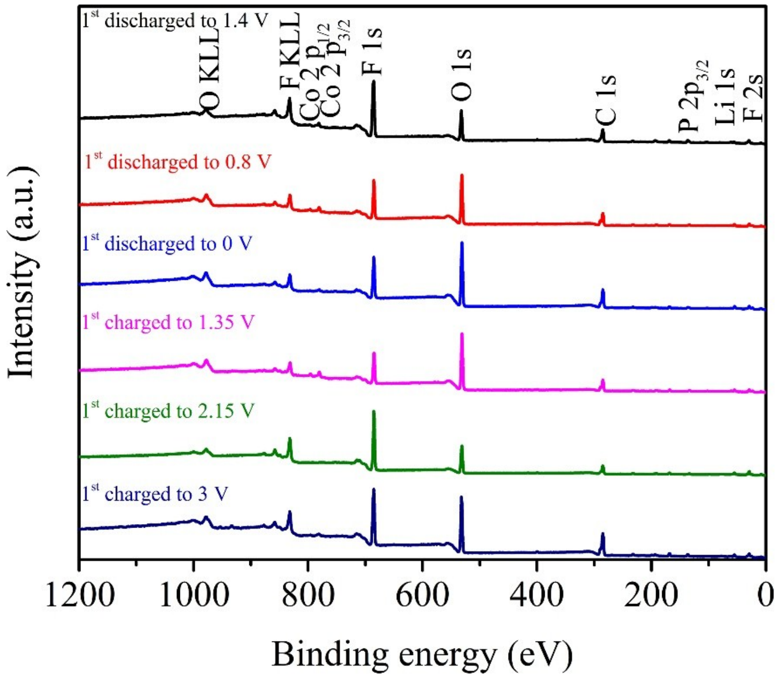

Fig. S12 Ex-situ XPS survey spectra of $Co_2(OH)_2CO_3$/rGO electrodes at different states.

Table S1. The fitted parameters of the $Co_2(OH)_2CO_3$/rGO electrodes from the equivalent electrical circuit.

Element	**before cycling**		**After 1th cycles**		**After 100th cycles**	
(Unit)	**Value**	**Error (%)**	**Value**	**Error (%)**	**Value**	**Error (%)**
Re (Ω)	3.257	1.9628	3.55	2.4454	9.741	3.3817
CPE-T(F)	8.9518E-6	5.0651	4.4669E-5	9.0629	2.4835E-4	8.1796
CPE-P	0.84313	0.61489	0.73224	1.2453	0.48186	1.9078
R_{ct} (Ω)	112.8	0.97801	33.31	1.4303	62.97	1.7624
Z_W (Ω)	246	4.0756	49.08	6.4497	39.92	10.31

Table S2. Comparison of structural characterization and electrochemical performance of the recent reports on the high performance anode materials for LIBs.

Morphology	Composite	Current ($A\ g^{-1}$)	Voltage Range (V)	Mass (g/cm^{-1})	Capacity retention after n cycles	Ref.
3D layered nanocubes	$Ni(HCO_3)_2$/rGO	10	0.01-3	1-1.3	803 mA h g^{-1} (n=2000)	Chem. Sci.[1]
Nanostructured porous	$MnCO_3$ spheres	5	0.01-3	-	510 mA h g^{-1} (n=2000)	Nanoscale [3]
$Mn_xCo_{1-x}CO_3$/rGO	$Mn_{0.7}Co_{0.3}CO_3$/rGO	2	0.01-3	-	901 mA h g^{-1} (n=1500)	Adv. Funct. Mater.[4]
Nanoparticals	MgH_2/graphene	2	0.01-3	-	395 mA h g^{-1} (n=1000)	ACS nano [5]
Nanosheets	MoS_2/graphene	1	0.01-3	~1	1250 mA h g^{-1} (n=150)	Adv. Energy Mater.[6]
Layer-by-layer	Co_3O_4/graphene	0.16	0.01-3	-	1502 mA h g^{-1} (n=300)	Angew. Chem. Int. Ed.[7]
Microporous polymers	poly(3,3′-bithiophene)	0.5	0.05-3	-	663 mA h g^{-1} (n=1000)	Adv. Funct. Mater.[8]
Liquid metal	Sn-Ga alloy	4	0.005-3	-	400 mA h g^{-1} (n=4000)	Energy Environ. Sci.[9]
3D nanoporous	SiGe	1	0.1-1	-	1158 mA h g^{-1} (n=150)	ACS Nano [10]
Hollow nanoparticles	CoO@BNG nanotubes	1.75	0.01-3	0.54-0.65	400 mA h g^{-1} (n=480)	Adv. Mater.[11]
Yolk–double Shell spheres	$NiCo_2V_2O_8$	1	0.01-1.5	0.8-1	1228 mA h g^{-1} (n=500)	Angew. Chem. Int. Ed.[12]
Nanowires	$Co_2(OH)_2CO_3$/rGO	10	0.01-3	1.2±0.2	550 mA h g^{-1} (n=5000)	**Current work**

References

1. Y. Dong, Y. Ma, D. Li, Y. Liu, W. Chen, X. Feng and J. Zhang, *Chem. Sci.*, 2018, **9**, 8682-8691.
2. Y. Dong, D. Li, C. Gao, Y. Liu and J. Zhang, *J. Mater. Chem. A*, 2017, **5**, 8087-8094.
3. W. Kang, D. Y. Yu, W. Li, Z. Zhang, X. Yang, T. W. Ng, R. Zou, Y. Tang, W. Zhang and C. S. Lee, *Nanoscale*, 2015, **7**, 10146-10151.
4. R. Zhang, X. Huang, D. Wang, T. K. A. Hoang, Y. Yang, X. Duan, P. Chen, L.-C. Qin and G. Wen, *Adv. Funct. Mater.*, 2018, **28**, 1705817.
5. B. Zhang, G. Xia, D. Sun, F. Fang and X. Yu, *ACS Nano*, 2018, **12**, 3816-3824.
6. G. Wang, J. Zhang, S. Yang, F. Wang, X. Zhuang, K. Müllen and X. Feng, *Adv. Energy Mater.*, 2018, **8**, 1702254.
7. B. Jiang, Y. He, B. Li, S. Zhao, S. Wang, Y. B. He and Z. Lin, *Angew. Chem. Int. Ed.*, 2017, **56**, 1869-1872.
8. C. Zhang, Y. He, P. Mu, X. Wang, Q. He, Y. Chen, J. Zeng, F. Wang, Y. Xu and J.-X. Jiang, *Adv. Funct. Mater.*, 2018, **28**, 1705432.
9. Y. Wu, L. Huang, X. Huang, X. Guo, D. Liu, D. Zheng, X. Zhang, R. Ren, D. Qu and J. Chen, *Energy Environ. Sci.*, 2017, **10**, 1854-1861.
10. Y. Yang, S. Liu, X. Bian, J. Feng, Y. An and C. Yuan, *ACS Nano*, 2018, **12**, 2900-2908.
11. H. Tabassum, R. Zou, A. Mahmood, Z. Liang, Q. Wang, H. Zhang, S. Gao, C. Qu, W. Guo and S. Guo, *Adv. Mater.*, 2018, **30**, 1705441.
12. Y. Lu, J. Nai and X. W. D. Lou, *Angew. Chem. Int. Ed.* , 2018, **57**, 2899-2903.